Polarization observables in $\pi\vec{d}$ elastic scattering: Analyzing powers T_{20} and τ_{21}

C. R. Ottermann, E. T. Boschitz, W. Gyles, W. List, R. Tacik, and M. Wessler
Kernforschungszentrum Karlsruhe, Institut für Kernphysik and Institut für Experimentelle Kernphysik, der Universität Karlsruhe, D-7500 Karlsruhe, Federal Republic of Germany

S. Mango, B. van den Brandt, and J. A. Konter
Schweizerisches Institut für Nuklearforschung, CH-5234 Villigen, Switzerland

D. R. Gill and G. R. Smith
TRIUMF, The University of British Columbia, Vancouver, British Columbia, Canada V6T 2A3
(Received 2 May 1988)

The tensor analyzing power T_{20} and the composite observable $\tau_{21} \equiv T_{21} + \frac{1}{2}(T_{22} + T_{20}/\sqrt{6})$ were measured at incident pion energies of 256 and 294 MeV, in an angular range between 90° and 172°, using a tensor-polarized deuteron target. The experimental procedure and data analysis techniques are discussed extensively. Comparisons are made with predictions from different three-body theories.

I. INTRODUCTION

There are a number of reasons why the study of the NN-πNN system is of considerable interest in nuclear and particle physics. From the nuclear physics point of view, it is the simplest few-body system in which conventional meson exchange theories can be rigorously tested. A thorough knowledge of the range of validity of these theories is a prerequisite for the understanding of the interaction of pions with nuclear matter. From the intermediate energy physics point of view, the πNN system provides a unique opportunity of investigating the interaction between a nucleon and a baryon in an elementary way. Nuclear structure effects tend to complicate related studies in nuclei, as in the case of the investigation of the ΔN interaction in π-nucleus scattering, or the determination of the ΛN or ΣN interaction in hypernuclei. Next, there is the possibility of the existence of dibaryon resonances. The observation of such exotics in the NN-πNN system would be quite exciting for particle physics. Finally, the question of charge symmetry breaking has been addressed in several $\pi^{\pm}d$ scattering experiments with the hope of extracting some information on quark masses. Therefore, it is not surprising that a considerable theoretical effort has been devoted to this system in the past 10 years.

Among the various πNN reaction channels, πd elastic scattering has been studied most extensively. This may be due to the apparent simplicity of this scattering process. The differential cross section at forward angles is well described by the impulse approximation. Only at large angles, where the cross section has dropped by 2 orders of magnitude, are effects due to multiple scattering and absorption important. Since the early calculation by Pendleton[1] in 1963, the theoretical developments have gone far beyond the Watson or Glauber type of multiple-scattering calculations.

Two theoretical approaches have emerged over the past few years. One is the coupled NN-πNN theory based on the Faddeev formulation.[2-5] The other is the coupled NN-$N\Delta$ theory based on nucleon-nucleon force models.[6,7] These calculations have reached a high degree of sophistication. However, there are still a number of open problems. Some of these are the importance of relativity, "off-shell" effects, heavy meson exchange, higher partial waves in the πN and NN input to the calculations, the importance of $N\Delta$ or $\Delta\Delta$ dynamics, and the correct inclusion of the coupled pion absorption channel (related to the treatment of the P_{11} πN t matrix in the πd calculation). These latter two problems will be discussed in further detail below.

On the experimental side, systematic investigations became possible with the advent of the pion factories. The first precision measurement of the $\pi^{\pm}d$ total cross section by Pedroni *et al.*[8] was followed by accurate measurements of the differential cross section by Gabathuler *et al.*[9] This measurement was extended to higher energies by Minehart *et al.*,[10] and to larger scattering angles by Stanovnik *et al.*[11] and Ottermann *et al.*[12] A comparison of the cross-section data with different theoretical predictions showed good agreement at forward angles, but there were systematic discrepancies at large angles, for pion bombarding energies above 180 MeV. In the years following, the vector analyzing power iT_{11} was measured by Smith *et al.*[13] over a large angular and energy range utilizing a vector polarized deuteron target. Again, systematic deviations from the theory were found above 180 MeV. The persistent failure of the theories to reproduce the differential cross section data at large angles, and the vector analyzing power at forward angles, indicated that some important dynamics may be missing in the conventional calculations. There were attempts to attribute this

missing dynamics to contributions from dibaryon resonances.[14,15] However, it was not possible to remove the discrepancies in cross section and vector polarization simultaneously in this way. Recently, the effects of short-range ΔN interactions were studied in order to attempt to explain the discrepancies between theory and experiment.[16] It is gradually becoming apparent that important contributions involving Δ components are missing in the conventional theories.[17]

At almost the same time as iT_{11} was being measured at the Swiss Institute of Nuclear Research (SIN), experiments to determine the tensor polarization $t_{20}^{\rm lab}$ of the recoil deuteron were underway at LAMPF.[18,19] These data revealed a new theoretical problem.

One of the developments in the course of the steady refinement of πNN theory was to provide a unified description of all reaction channels. In this description, the pion absorption and the pion elastic scattering channels were coupled via the P_{11} πN amplitude. Field theoretical considerations led to a model in which this amplitude was divided into "pole" and "nonpole" parts, both of which could be large, their sum, however, had to be small because of the on-shell behavior of the P_{11} πN amplitude at pion energies up to 300 MeV.[21,22] It now came as a surprise that this new version of the NN-πNN Faddeev theory disagreed markedly with the $t_{20}^{\rm lab}$ data; while theoretical calculations which either neglected the π-absorption channel altogether[23] or kept the individual pole and nonpole terms small[24] agreed quite well. This "P_{11} puzzle" is an interesting problem. It arises because, in πd scattering in the intermediate NN state, the pole term is Pauli blocked for certain partial waves, and the tensor polarization $t_{20}^{\rm lab}$ at large angles becomes very sensitive to the exact way in which the P_{11} πN t matrix is split.

In order to clarify the existing problems in the theoretical description of πd scattering a model independent approach is needed. In the energy range of the $\Delta(3,3)$ resonance too many partial waves are involved for a theory-independent partial wave amplitude analysis, but a helicity amplitude reconstruction may be feasible. πd elastic scattering can be described by four complex helicity amplitudes. This means that up to a common phase at least seven independent observables must be determined and this is possible with present technologies.

Two years ago a tensor-polarized deuteron target, suitable for πd scattering in the $\Delta(3,3)$ energy range, became available and a Karlsruhe-SIN-TRIUMF collaboration embarked on a program to measure the c.m. tensor observables T_{20}, T_{21}, and T_{22} in the backward hemisphere at five pion energies between 134 and 294 MeV. The first results from TRIUMF were published in Refs. 25 and 26. An extensive paper has been published.[27] In the present publication we report on the SIN part of the collaboration. The measurements were performed with two different experimental setups in two beam periods. In this paper we describe the measurement of T_{20} and τ_{21} and in a subsequent paper that of τ_{22} and iT_{11}. There we shall also show the consistency between the previous tensor-polarization data and the present tensor analyzing power measurements.

II. THE EXPERIMENT

A. Method

In principle, there are two ways of measuring polarization observables in πd elastic scattering. In one method, the polarization of the final-state deuteron is determined with a nuclear reaction in a calibrated polarimeter, in a double-scattering experiment. In the other method, the analyzing power of the initial-state polarized deuteron is measured in a single-scattering experiment.

The first technique has several drawbacks. The low event rate of a double-scattering experiment limits the number of data points which can be measured in a reasonable time. Also, the energy and angular range over which it can be applied is restricted. At low incident pion energies, and for small pion scattering angles, the recoil deuterons do not have sufficient energy to escape from the target. At high bombarding energies, and for large pion scattering angles, the recoil deuteron energy must be degraded in order to match that for which the analyzing power of the polarimeter is known. This can cause problems due to energy straggling and multiple scattering. In addition, the first method requires special care because of the distribution in energy and angle of the scattered deuterons as well as the presence of other particle types incident on the polarimeter. In spite of these difficulties, the tensor polarization t_{20} was measured for several energies at LAMPF (Refs. 18 and 19) and TRIUMF (Ref. 20) before suitable tensor-polarized deuteron targets were available.

The vector analyzing power iT_{11} was determined with the second technique, by scattering pions from a polarized deuteron target.[13] More recently, the analyzing power T_{20} and the composite observable τ_{21} were measured[25,26] with a tensor-polarized deuteron target.[28,29] This method of using polarized targets is also not without problems. For precise measurements, the target must be highly polarized, preferably with $p_z \geq 0.40$. This may require polarizing times of up to 8 h. Polarized targets contain nuclei other than deuterons, and therefore a careful background subtraction is needed. Polarized targets employ high magnetic fields which affect the particle trajectories. These magnetic fields must be very homogeneous ($\Delta B/B \leq 10^{-4}$) over a certain volume in order to polarize the target. This limits the target size, in our case to about 4 cm^2, and thus the pion beams used must be well focused.

A great advantage of the polarized target method over the double-scattering technique is that, besides some minor restrictions in the angular range due to the geometry of the superconducting magnet coils, there is no limitation in scattering angle and energy over which experiments can be performed. This is important for collecting a complete data set. Also, data acquisition in single-scattering experiments is much faster, especially since several angles may be measured simultaneously with a multidetector setup. Another important advantage of the polarized target method lies in the fact that the measurement of the cross sections and the determination of the polarization are completely decoupled.

The differential cross section for scattering a pion from a polarized deuteron target, $\sigma^{\rm pol}$, can be expressed in terms of the cross section for scattering from an unpolarized target, σ^0, as

$$\sigma^{\rm pol}=\sigma^0(1+a_{11}\cdot iT_{11}+a_{20}\cdot T_{20}+a_{21}\cdot T_{21}+a_{22}\cdot T_{22}) , \tag{1}$$

where

$$a_{11}=\sqrt{3}p_z\sin\alpha\cos\beta ,$$

$$a_{20}=\frac{p_{zz}}{\sqrt{2}}\frac{(3\cos^2\alpha-1)}{2} ,$$

$$a_{21}=\sqrt{3}p_{zz}\sin\alpha\cos\alpha\sin\beta ,$$

$$a_{22}=-\frac{\sqrt{3}}{2}p_{zz}\sin^2\alpha\cos 2\beta .$$

iT_{11} is the vector analyzing power and T_{20}, T_{21}, and T_{22} are the tensor analyzing powers which are to be measured. Their contributions are determined by the coefficients a_{11}, a_{20}, a_{21}, and a_{22}, which are functions of the target vector polarization p_z, the corresponding tensor polarization p_{zz}, and the angles α and β. α is the polar angle between the incident pion beam direction ($\hat{k}_{\rm in}=\hat{z}$) and the quantization axis, which is the direction of the target magnetic field. β is the angle between the y axis ($\hat{y}=\hat{k}_{\rm in}\times\hat{k}_{\rm out}$) and the projection of the quantization axis on the x-y plane ($\hat{x}=\hat{y}\times\hat{z}$). Note that due to the way in which the target is polarized, in our case p_{zz} is always positive, whereas $p_z>0$ for positive target polarizations and $p_z<0$ for negative ones.

With a proper choice of angles α and β, measured polarized and unpolarized cross sections can be used to determine analyzing powers. For example, with $\alpha=0°$ (β undefined) T_{20} can be determined directly. By choosing $\beta=90°$ and $\alpha=45°$ one can eliminate the a_{11} coefficient, and enhance the contribution of a_{21} with respect to a_{20} and a_{22}. This is what was chosen for the measurement of

$$\tau_{21}\equiv T_{21}+\tfrac{1}{2}T_{22}+T_{20}/\sqrt{6} .$$

Note that another possible choice would have been $\alpha=54.7°$, which would have eliminated the T_{20} term completely. This configuration was not preferable, however, due to complications arising from the geometrical bounds of the polarized target magnet. Under the two above-mentioned conditions, Eq. (1) can be rewritten as

$$\sigma^{\rm pol}=\sigma^0\left[1+\frac{1}{\sqrt{2}}p_{zz}T_{20}\right], \quad \alpha=0°,\ \beta \text{ undefined} ,$$

$$\sigma^{\rm pol}=\sigma^0\left\{1+\frac{\sqrt{3}}{2}p_{zz}\left[T_{21}+\frac{1}{2}\left[T_{22}+\frac{T_{20}}{\sqrt{6}}\right]\right]\right\},$$

$$\alpha=45°,\ \beta=90° .$$

One can see that for the determination of the polarization observables only the ratio $\sigma^{\rm pol}/\sigma^0$ must be measured for a known tensor-polarization p_{zz}. Thus, in principle, only one polarity is needed for these measurements, as was the case in recent TRIUMF experiments. However, the knowledge of both ratios σ^+/σ^0 and σ^-/σ^0 provides redundant information which can be used to test the reliability of the determination of the target polarization. It can also be used to check the alignment of the experimental setup, and, in the case of a misalignment, would allow one to correct for unwanted iT_{11} contributions.

B. The polarized deuteron target

Target vector (p_z) and tensor (p_{zz}) polarizations are defined as

$$p_z=n^+-n^- ,$$

$$p_{zz}=n^++n^--2n^0=1-3n^0 ,$$

with

$$n^++n^0+n^-=1 ,$$

where n^+, n^0, and n^- stand for the populations of the deuteron magnetic substates with $m=+1$, 0, and -1, respectively. Under certain assumptions, the two polarizations are related to each other through the relation

$$p_{zz}=2-(4-3p_z^2)^{1/2} . \tag{2}$$

The first assumption is that the populations of the three magnetic substates can be described by a Boltzmann distribution. This is known as the "equal spin temperature" assumption, and is considered reasonable for deuterated alcohols.[32] The other assumption is that one can neglect the effects of the deuteron quadrupole moment. This seems reasonable, since the quadrupole interaction energy is characterized by a frequency of the order of 20 kHz,[33] whereas the deuteron Larmor frequency is 16.6 MHz for a magnetic field of 2.5 T.

All of the early measurements of the vector analyzing power iT_{11} in various πd reaction channels[13,30,31] were performed with a polarized target employing a ^{3}He refrigerator, and therefore operating at about 0.5 K. The resulting vector polarization of the deuterons was typically $p_z=0.18$. For measurements of the tensor analyzing power, a much larger vector polarization is needed in order to obtain a sizable tensor polarization p_{zz}. For example, according to Eq. (2), a vector polarization of 0.40 is required in order to obtain a tensor polarization of 0.13. Such large vector polarizations can only be achieved with sufficient cooling power at temperature well below 0.5 K. Therefore, a new polarized deuteron target was constructed at SIN, the main component of which is a top-loading ^{3}He/^{4}He dilution refrigerator with a cooling power of about 4 mW at a temperature of 0.3 K, and a base temperature ≤ 0.05 K. The target material consisted of deuterated propandiol [a mixture of $C_3D_6(OD)_2$ and $C_3D_6(OH)_2$, 92% deuterated], doped with Cr^V complexes, in the form of beads with a diameter of about 1 mm, immersed in the liquid ^{3}He/^{4}He mixture. The beads were contained in a brass cell (wall thickness 0.1 mm) with dimensions $5\times18\times18$ mm^3. The filling factor was estimated to be 0.5. The pickup coil of the NMR system, a printed circuit on a 0.2 mm thick glass fiber reinforced Teflon plate, was in the midplane of the cell. The inner

brass cell was surrounded by a 0.5 mm thick $^3He/^4He$ layer, contained in an additional 0.1 mm thick brass cell ($6\times19\times19$ cm^3) and a stainless steel cell (wall thickness 0.1 mm) with dimensions $7\times20\times20$ mm^3, which separated the dilution refrigerator from the isolation vacuum of the scattering chamber (diameter 30 cm). Aluminized Kapton windows (0.125 mm thick) in the scattering chamber permitted the detection of scattered pions and deuterons over a large angular range.

The dynamic polarization of the target was produced by irradiating the deuterated propandiol with microwaves while the target magnetic field was kept at 2.5 T and the temperature at about 0.3 K. Positive and negative polarizations were obtained with slightly different microwave frequencies (69.86 GHz for p_z^+ and 70.20 GHz for p_z^-), and did not involve reversing the polarity of the magnetic field. This avoids changes in the experimental conditions for the measurement of the relative cross sections. The deuteron polarization was determined by NMR techniques which will be described below. As soon as a sufficiently large polarization was achieved, the microwave power was turned off, and the polarization was "frozen" at temperatures of about 0.05 K. Operating in such a "frozen spin mode" reduces random variations in the polarization value, which may originate from drifts of the microwave frequency during the dynamical polarization process. Also, under these conditions one can lower the magnetic field to some "holding" value (typically $\frac{1}{3}$ of $B_{\max}$) without significantly decreasing the decay time of the polarization. This is more than 400 h at normal field (2.5 T) and about 150 h for holding fields of 0.83 T. This time is still large compared to a typical data acquisition period of 4–8 h. The reduced magnetic field also has less effect on the trajectories of the incoming and outgoing particles, and thus simplifies the setup.

In addition to deuterons, there are other nuclei present in the target material and cell. Most of the background events arising from these nuclei can be easily separated from the πd elastic scattering events. Some quasifree πd scattering events cannot be distinguished, however, and a seperate background measurement is required. Previous measurements indicate that about 75% of the background events originate from the $^3He/^4He$ mixture and the walls of the target cells. Thus, only the deuterated propandiol was replaced by a slab of CH_2 ($2.7\times18\times18$ mm^3) for the background measurement. The thickness of the CH_2 was chosen in such a way as to match the number of carbon nuclei to the carbon and oxygen nuclei in the propandiol target.

The deuteron polarization was determined by measuring the absorptive part of the nuclear magnetic resonance (NMR) signal detected with a constant current Q meter. The output of an oscillator, swept in 32 ms with a repetition rate of 0.3 Hz between 16.33 and 16.70 MHz, was fed into a resonance circuit, which consisted of a pickup coil, positioned in the median plane of the target container, connected to a Ga-As variable capacitor diode (Varicap) by a section of 50 Ω coax cable 18 cm long. The Varicap was directly connected to the input of a field-effect transistor (FET) amplifier, both of which were capable of operating at temperatures of ~0.7 K. This circuit was kept at resonance at each frequency by varying the capacitance of the Varicap synchronously with the frequency sweep. In this way, frequency dependent distortions of the NMR signal due to the high Q available were kept minimal. The high-frequency voltage across the resonant circuit was amplified and rectified before being sent to a 512 channel digital signal averager. The absolute magnitude of the vector polarization p_z was obtained from the deuteron NMR signals in two ways.

In the first technique the integral of the thermal equilibrium (TE) NMR signal was compared with that of the dynamically enhanced polarized signal. From this ratio the target polarization was calculated. Typical TE and dynamical NMR signals are shown in Fig. 1. The TE polarization was calculated from the known temperature T and the magnetic field B according to

$$p_z(\mathrm{TE})=\frac{4\tanh(\mu B/2kT)}{3+\tanh^2(\mu B/2kT)}\simeq\frac{2}{3}\frac{\mu B}{kT},$$

where $\mu=2.703\times10^{-14}$ MeV/T is the deuteron magnetic moment, and k is the Boltzmann constant. In this experiment ($B=2.5$ T and $T=0.65$ K) a value of $p_z(\mathrm{TE})=0.000\,80$ was obtained. The polarization of the dynamically polarized target can then be deduced directly from

$$p_z(\mathrm{dyn})=\frac{A(\mathrm{dyn})}{A(\mathrm{TE})}\times p_z(\mathrm{TE}),$$

where $A(\mathrm{dyn})$ is the integral of the dynamical NMR signal and $A(\mathrm{TE})$ the corresponding integral of the thermal equilibrium NMR signal. In this method one must ensure that the gain of the NMR detection system is linear over the range of amplification required for the TE and the dynamical polarization signals. Also the shape of the background underneath the NMR signal, due to electron-

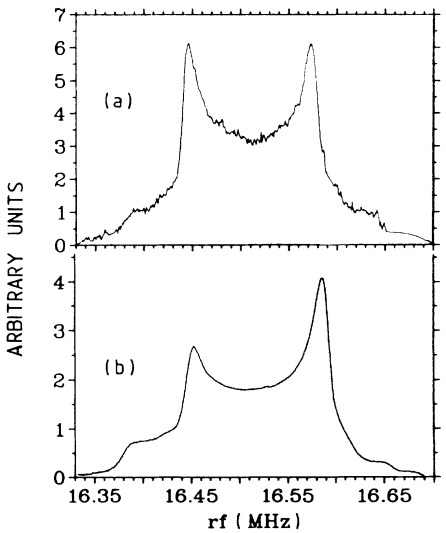

FIG. 1. (a) Typical thermal equilibrium NMR signal, corresponding to a vector polarization of $p_z=0.000\,80$. (b) Dynamically enhanced NMR signal, $p_z=0.417$.

ic noise, must be well known and properly subtracted. The uncertainty in the determination of the TE signal (typically 5%) is mainly due to uncertainties in measuring the temperature. It enters as an absolute normalization error in the uncertainty of the analyzing power. During the experiment the TE signal was measured repeatedly, and consistent values were obtained.

The second technique uses the asymmetry of the doubly peaked deuteron NMR signal.[33] The hyperfine interaction of the deuteron quadrupole moment with the electric field gradients in the *C-D* and *O-D* bonds of the propandiol molecule shifts the energy levels of the deuteron magnetic substates. The amount of these shifts depends on the angle between the magnetic field direction and the axis of the bond. The angular variation separates and broadens the resulting pair of transitions. The vector polarization of the target can be obtained directly from the ratio R, according to

$$p_z = \frac{1-R^2}{1+R+R^2} ,$$

where R is defined as

$$R = \frac{\text{intensity}(m=-1 \leftrightarrow m=0)}{\text{intensity}(m=0 \leftrightarrow m=+1)} = \frac{\text{left peak area}}{\text{right peak area}} .$$

This technique is in principle superior to the former method since it avoids the difficult measurement of the very small thermal equilibrium NMR signal. However, the values extracted from this "ratio method" may depend on the specific shape of the NMR signal, which is given by the target material, solid-state effects in the target, and the characteristics of the NMR readout system. Also, a frequency independent gain over the frequency range of the NMR signal is required. If the background underneath the NMR signal is not well known, it becomes difficult to extract the correct asymmetry. In our analysis we followed the method discussed by Hamada,[33] in which the signal shape is represented by an analytic expression. The free parameters in this expression were optimized to reproduce the measured signal shape. Most parameters were found to be constant for all NMR signals measured during this experiment. Thus, it was only necessary to fit the amplitude, the asymmetry, and the background (a polynomial up to third order) for the individual spectra. In Fig. 2(a), a dynamical signal (solid line) and the corresponding result of the fitting procedure (dashed line) are illustrated. Figure 2(b) shows the decomposition of the fitted signal into its two components, from which a polarization of $p_z = -0.482$ was determined. A systematic uncertainty in the value of p_z arises from the determination of the background. The error is typically 4%.

The polarization values for p_z obtained with both methods agreed well. Therefore the mean value of both methods was taken as the final result for the vector polarizations. The estimated absolute uncertainty in the final values is 4%. The relative error for the determination of positive versus negative polarizations is ±2.5%. The maximal vector polarization achieved during this experiment was −0.48, after a polarization time of about 12 h. For more typical polarization times of about 4 h, values

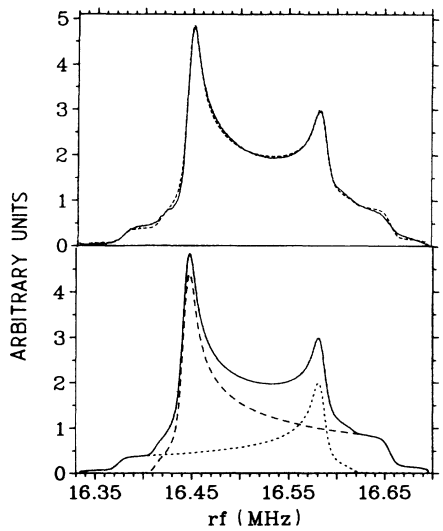

FIG. 2. Dynamical signal for a vector polarization of $p_z = -0.482$. (a) The solid line represents the measured NMR signal, the dashed one the best fit obtained with the procedure described in the text. (b) The solid line corresponds to the dashed one in (a). The dashed and dotted lines are the individual contributions of the $m=-1 \leftrightarrow m=0$, and $m=0 \leftrightarrow m=+1$ transitions as obtained from the fit.

ranged between 0.39 and 0.44, for both polarities. From the vector polarization p_z, the tensor polarization p_{zz} is calculated using Eq. (2). The uncertainty Δp_{zz} is given by

$$\frac{\Delta p_{zz}}{p_{zz}} = \frac{4-p_{zz}}{2-p_{zz}} \cdot \frac{\Delta p_z}{p_z} \simeq 2 \cdot \frac{\Delta p_z}{p_z} .$$

C. The pion beam

Our experiments were performed with pions from the $\pi M1$ beam line at the Swiss Institute of Nuclear Research. We used the multicounter time of flight (TOF) spectrometer illustrated in Fig. 3, which has been used for many of our previous πd experiments.[12,13,30,31] It was placed 1.5 m downstream of the usual channel focus. This increased the beam spot to 1.2 cm FWHM, which was still comparable to the target size. The beam divergence in the scattering plane was less than ±1°, while perpendicular to it, it was less than ±3°. The electrostatic separator in the beam line removed most incoming protons. The remaining few were eliminated by pulse height discrimination in a thin dE/dx scintillation counter in the beam. Muons and electrons originating from the pion production target and from pion decays near the beginning of the beamline (length 22.5 m) were separated from the pions by time of flight. The number of muons from pion decay close to the scattering target were estimated by Monte Carlo methods to be less than 1%, and were neglected in the determination of the relative cross sections. The beam momentum at the target center was determined to within ±0.3% from the magnetic field in the second bending magnet in the $\pi M1$ beamline,[8] and

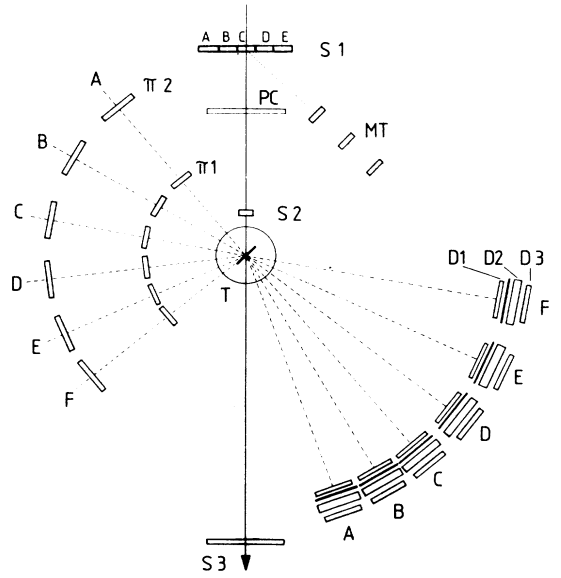

FIG. 3. Schematic view of experimental setup: $S1$ is a five element hodoscope; PC a multiwire proportional chamber; $S2$ the beam defining counter; T the polarized target; MT a monitor telescope; $\pi 1$ and $\pi 2$ are the pion counter telescope detectors; D_1, D_2, and D_3 are the deuteron counter assembly. The solid lines between counters D_1 and D_2 are the iron degraders. $S3$ consists of four adjacent counters.

the calculated energy loss of the pions in the material upstream of the target center. Because of the smooth variation of the analyzing powers with energy, high momentum resolution was not required in this particular experiment. Therefore, the full momentum band of the channel ($\Delta p/p = \pm 1.5\%$) was accepted. Typical pion intensities were 5×10^6 π^+/s, allowing the number of incident pions to be counted directly.

The incoming pion beam was detected by two plastic scintillators $S1$ and $S2$ (see Fig. 4). The beam spot on the target was defined by the counter $S2(2\times 10\times 15$ mm^3), positioned 20 cm upstream from the target in the converging beam. The scintillation counter hodoscope $S1$

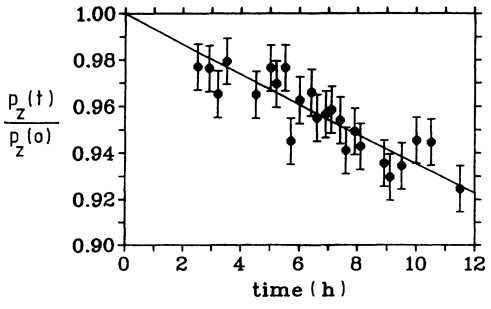

FIG. 4. Decay of the target polarization in frozen spin mode. The line represents an exponential fit to the polarization values p_z. From this the mean life of the target polarization, $\tau = 150$ h is calculated for the holding field $B = 0.83$ T.

consisted of five elements ($S1_A, \ldots, S1_E$, $2\times 10\times 100$ mm^3 each). It was positioned 1.5 m upstream from the target, and monitored the direction of the incident pion beam, its distribution in the scattering plane, and the incident pion rate. An incident pion event was defined by the following coincidence requirement:

$$\text{BEAM} = \text{rf}\cdot S2\cdot\overline{S2}\cdot\sum(S1_i\cdot\overline{S1_i}) \quad (i = A, \ldots, E) .$$

The veto signals $\overline{S2}$ and $\overline{S1_i}$ $(i = A, \ldots, E)$ were obtained from an upper level pulse height discrimination in the respective counters. They rejected the few protons which passed through the channel electrostatic separator. Multiple pion events per beam burst (length 2 ns) were not rejected by the upper threshold and were counted as a single pion event. This effect was corrected for, as will be described below. The radio frequency signal (rf) of the SIN cyclotron (50 MHz) was used in the BEAM coincidence to create a TOF window to reject muons and electrons in the pion beam. The time definition of the BEAM coincidence was determined by the $S2$ counter. The BEAM coincidence accepted 60% of the total incoming pion flux. The remaining 40% missed the $S2$ counter.

D. Pion-deuteron detection system

In Fig. 3, a schematic layout of the pion-deuteron detection system is shown. It consists of six scintillation counter telescopes ($\pi_A, \ldots, \pi_F$), used to detect the scattered pions, and six associated scintillation counters, used to detect the recoil deuterons in coincidence.

For the T_{20} measurement, the target magnetic field deflects the pion and deuteron trajectories out of the scattering plane. Since the T_{20} measurement is independent of the angle β, i.e., there is rotational symmetry around the beam axis, we kept pion counters in the horizontal plane, but raised the deuteron counters by an appropriate amount. For the τ_{21} measurements, the axis of the target magnetic field was in the horizontal plane, but at an angle of 45° to the incident beam. The scattering plane was defined by the incoming beam direction and the fixed magnetic field direction. In this case the magnetic field distorts the pion and the deuteron trajectories in such a way that each pion and each deuteron counter had to be positioned out of the horizontal plane at different azimuthal angles.

The pion telescopes consisted of two scintillation counters. The first one, π_1, was $0.3\times 6\times 16$ cm^3, at a distance of 0.5 m from the target. The second counter, π_2, was $0.5\times 10\times 30$ cm^3, at a distance of 1 m from the target. It defined the solid angle of 29.6 msr of the pion telescope, and the angular acceptance of 5.7° in the scattering plane. The angular acceptance of the two counters together was such that only particles originating near the target region were counted. A scattered pion event was defined by

$$\text{PION}_i = (\pi_1\cdot\pi_2) \quad (i = A, \ldots, F) ,$$

where the timing was determined by the signal π_2. This signal was obtained, via a mean timer, from the output of

two photomultipliers that view the scintillator π_2 from both ends.

The detectors for the recoil deuterons consisted of three closely spaced scintillator counters, D_1 ($0.5\times10\times40$ cm^3, 1.3 m away from the target), followed by D_2 ($2.0\times11\times42$ cm^3) and D_3 ($0.5\times10\times40$ cm^3). The three counters serve as a ΔE-E-veto system for particle identification and background suppression. The design of these counters was optimized with Monte Carlo methods to ensure that the solid angle they covered was larger than that of the corresponding pion counter telescopes. The D_1 counter served as a ΔE detector, except for deuterons with $T_d < 30$ MeV which were stopped. In most cases, deuterons would stop in the D_2 counter. To compensate for the variation in deuteron energies at different angles, a degrader of appropriate thickness was placed between D_1 and D_2. The spacing between these two counters was less than 1 cm to avoid deuterons straggling out of D_1 and missing D_2. Iron was chosen as the degrading material. The veto counter D_3, directly behind D_2 rejected protons from quasifree scattering reactions.

A deuteron event is defined by

$$\text{DEUTERON}_i=(D_1\cdot\overline{D_3})_i \quad (i=A,\ldots,F)\ ,$$

where the timing is determined by the signal D_1 which originates from the mean time of the signals from two photomultipliers, as was the case for π_2. The D_2 signal was not included in the coincidence requirement to avoid the rejection of deuterons which stopped in D_1.

The final definition of a genuine πd scattering event was the coincidence

$$\text{EVENT}_i=\text{BEAM}\cdot\text{PION}_i\cdot\text{DEUTERON}_i \qquad (i=A,\ldots,F)$$

for each of the associated pion-deuteron arms. In this coincidence the BEAM signal defined the timing. It was therefore possible to reject that part of the quasifree πp background which was well separated by TOF from the πd elastic events. The intrinsic timing resolution was better than 0.7 ns. The kinematic broadening in the πd elastic reaction, and the different energy losses and straggling effects increased this resolution by a factor of 2–3. The EVENT signals were fed into a CAMAC pattern unit, the starts of the CAMAC time-to-digital converters (TDC), and the gates of the CAMAC analog-to-digital converters (ADC). The TDC's were stopped by the individual signals of the scintillators or mean timers. Finally the EVENT signal triggered a CAMAC readout cycle.

E. Beam alignment and stability

The target cell and the magnet coils of the polarized target were positioned with respect to its vacuum chamber to an accuracy of 1 mm and 0.5°. After final assembly of the target these positions were checked with x-ray scans. The beam counters and the target chamber were aligned with respect to the pion beam line to within 1 mm using optical methods. The distances between the pion and deuteron detectors and the target were known within 5 mm. The uncertainty in the angular positions of the detectors was 0.3°. The angular orientation of the target in the horizontal and vertical planes was determined with a laser beam which was reflected from a mirror plate attached to the chamber. The accuracy was 0.2°. In the cases where the target was rotated by 45° with respect to the incoming beam (τ_{21} measurement) the detector $S2$ was rotated by the same amount, in order to ensure that the beamspot, defined by this counter, was still smaller than the target. Therefore the T_{20} and τ_{21} measurements were performed with the same BEAM defining system.

In order to verify the alignment of the $S2$ counter with respect to the target, the $S2$ counter was moved vertically and horizontally, and the ratio of πd elastic scattering events to BEAM was maximized. No major deviations were found between the final position of $S2$ and its location defined by the optical alignment.

In order to ensure that the experimental conditions did not change within a series of relative cross-section measurements, the distribution and direction of the incident pion beam were monitored continuously with several methods. As an indicator for changes in the BEAM coincidence the ratios $\sum S_i$/BEAM and S_2/BEAM were monitored. The BEAM rate was also compared with the proton rate at the pion production target. In addition, a three-element counter telescope MT viewed the counter $S1$ at an angle of 45° relative to the incident beam direction, from above, and served as an additional beam rate monitor. The horizontal and vertical beam profiles were monitored by a multi wire proportional chamber (PC). The distribution of the incoming beam was also measured by the fivefold $S1$ counter, and recorded. The ratio

$$(S1_A+S1_B-S1_D-S1_E)/S1_C$$

was found to be very sensitive to shifts of the center of gravity of the beam. In the case of the T_{20} measurement, where the target magnetic field has very little effect on the incoming pion beam, an additional counter array ($S3$) was used to monitor the beam position downstream of the target. This counter consisted of four square scintillators ($0.5\times10\times20$ cm^3), mounted quadratically in a plane perpendicular to the beam, 3.88 m downstream of the target. The segmentation into four quadrants permitted us to define a horizontal and vertical center of gravity of the pion beam. In order to be sensitive only to those pions which fulfilled the BEAM coincidence requirement, the signals of the individual quadrants were put in coincidence with the BEAM signal. Adding the count rates of two quadrants each, upper (U), lower (D), left (L), and right (R) count rates were calculated. Due to the large distance from the beam defining counter $S2$, very small deviations from the prealigned beam direction could be registered by the ratios $UD=(U-D)/(U+D)$ and $LR=(L-R)/(L+R)$.

The determination of T_{20} is very sensitive to misalignments of the beam. A simple calculation shows that the axis of the target magnetic field must be collinear with the pion beam direction to within 1° in the horizontal plane to eliminate significant contributions from the other analyzing powers. This was ensured in two ways.

After having aligned the polarized target chamber

mechanically with respect to the optical axis of the beamline, the direction of the target magnetic field was measured with a compass needle at several distances in the horizontal plane. Comparing these measurements with the known field map of the magnet, the target field orientation could be inferred to within 0.3°. In principle, this allows one to correct for target misalignments by rotating the target chamber. However, there are limitations in the accuracy of this method. For example, the length of the compass needle used averages over magnetic field lines. Also, there can be misalignment of the needle and the readout system. Although some of these difficulties can be overcome, a second, superior, method was employed. This involves the pion beam itself together with the quadrant counter $S3$. First, this counter was centered with respect to the pion beam, with the target magnetic field turned off. Then, the target magnetic field was turned on, and the target was rotated in the horizontal plane and tilted in the vertical plane in steps of 1° and 0.1°, respectively. These angles were measured accurately with a laser beam reflected from a mirror that was attached to the outside of the target chamber. We found that the $S3$ count rate ratio UD changed by 0.067 for each degree of horizontal rotation of the target, and LR changed by 0.093 for each degree change in the vertical tilt angle. Using this calibration, the target could be aligned with respect to the pion beam direction to within 0.05°. The final target position, determined in this way, was the same, within uncertainties, as that determined optically and with the needle method. The stability of the alignment was monitored during the entire T_{20} measurement by monitoring the UD and LR ratios for each individual run. In particular, the beam alignment was checked with this method whenever the magnetic field was turned off and on again to depolarize the target.

F. Data acquisition

The entire measurement for T_{20} and τ_{21} was subdivided in data taking cycles in order to eliminate systematic errors which may arise from electronic drifts over a long time. Each cycle consisted of a sequence of equally long measurements of σ^{pol}, σ^0, σ^0, and σ^{pol}. In total we measured between four and six cycles in the following sequence

$$(\sigma^+\sigma^0\sigma^0\sigma^-)(\sigma^-\sigma^0\sigma^0\sigma^+)(\sigma^+\sigma^0\sigma^0\sigma^-)\ldots .$$

In order to minimize the contribution of the statistical error in the cross section to the overall error in T_{20} and τ_{21}, a minimum of 10 000 πd elastic scattering events were accumulated and used in the determination of each cross section.

Because we operated the target in "frozen spin" mode, with a reduced target magnetic field, the data taking procedure was quite involved. First, the target was polarized in 4–8 h at the normal magnetic field of 2.5 T. Having achieved a sufficiently large polarization ($p_z > 0.40$) the microwave power was turned off, and consequently the target temperature dropped to 0.05 K. Still at normal field, an NMR signal was recorded for later detailed analysis. Next, the magnetic field was lowered to the holding field value of $B = 0.83$ T. The polarized cross section was then measured for several hours. At the end of the data acquisition the magnetic field was raised to its normal value and the NMR signals were recorded again. In Fig. 4 we show the results of many polarization measurements after different decay times. The decay time was determined by fitting an exponential curve to the data. For the measurement of the unpolarized cross section the magnetic field was lowered to zero to destroy the target polarization. This was done slowly (about 20 min) in order to avoid a quench of the superconducting magnet. Once the polarization was zero, the magnetic field was brought back up to the holding field value of 0.83 T again and data were collected for the unpolarized cross section under the same conditions as for the polarized ones.

III. DATA REDUCTION

A. Cross-section determination

As already discussed, the polarization observables are determined from the ratios of σ^{pol} and σ^0. The solid angle $\Delta\Omega$ and the number of target nuclei n_T, which normally are necessary to evaluate an absolute differential cross section, cancel in these ratios. Therefore the relative cross section σ for the πd elastic scattering reaction was obtained using the expression

$$\sigma = \frac{\text{YIELD}}{n_B \cdot \epsilon_{\text{CPU}}} ,$$

where YIELD represents the number of πd elastic events, n_B the corresponding number of incident pions and ϵ_{CPU} the computer efficiency. This was determined from the ratio $\epsilon_{\text{CPU}} = \text{LAMS/EVENTS}$, where EVENTS represents the total number of events, counted with a CAMAC scaler, and LAMS those events which were accepted by the computer. The number of incident pions was determined from $n_B = \text{BEAM} \times \eta$, where η is a correction factor which accounts for the multiple pions in a beam burst which were counted as a single incoming pion:

$$\eta = \frac{-\ln(1-\mu)}{\mu} ,$$

$$\mu = \frac{\text{no. of beam bursts containing at least one pion}}{\text{total no. of beam bursts}} .$$

A good approximation for μ was

$$\mu \frac{\sum S1_i}{rf} = \frac{\sum S1_i}{50\ \text{MHz}} .$$

For a typical $\sum S1_i$ rate of less than 10 MHz, the correction is less than 12%. The validity of this correction was successfully tested between 4.5 and 29.4 MHz by measuring the rate dependence of the cross section. Also, in order to guarantee that the beam rate stayed rather constant within a sequence of relative cross-section measurements, the incoming beam rate was counted by a rate meter, and data acquisition was interrupted when the beam rate dropped below 70% of the normal rate. Since polarized and unpolarized cross sections were measured with

roughly the same incident pion rates, this correction for multiple pions will cancel to a large extent anyway.

The YIELD of the πd events was determined in the following way. The deuterons were identified in a two-dimensional plot of the pulse heights of D_1 or D_2 vs the time of flight difference $D_1 - \pi_2$ (see Fig. 5). These deuterons were well separated from background protons, originating from quasifree πp and knockout reactions. A polygon was drawn around the deuteron events, and the events outside rejected. A small background from quasifree πd reactions remained inside the polygon, and was subtracted from the foreground, after being measured separately, with the use of a background target. Figure 6 shows a typical one-dimensional spectrum of the D_2 pulse height for a foreground run (solid line) and a background run (dotted line), normalized to the same number of incident pions, after employing the polygon cut. The quasifree πd background spectrum is structureless and matches the foreground on either side of the πd elastic peak. The background contribution was 8–21 %, depending on the scattering angle, beam energy, and target angle. The YIELD of the πd elastic scattering events was obtained by a straightforward integration of the πd peak after subtracting the background, taking into account the statistical uncertainties of the background measurements.

As mentioned above only relative cross sections are required for determining T_{20} and τ_{21}. However, absolute cross sections were calculated in order to test the reliability of the setup. Naturally, there are large uncertainties in this calculation, owing to the nature of a polarized target (beads as target material, magnetic field acting on the particle trajectories, straggling effects in the target cells, etc.). The absolute differential cross section is defined by

$$\frac{d\sigma}{d\Omega} = \frac{\text{YIELD}}{n_B \epsilon_{\text{CPU}} n_T \Delta\Omega \epsilon_{\text{corr}}} = \frac{\sigma}{n_T \Delta\Omega \epsilon_{\text{corr}}} .$$

In this expression $\Delta\Omega$ is the defining solid angle of the πd conjugate counter pair (29.6 msr). The effect of distortions, caused by the target magnetic field, on the solid angle, was estimated to vary between 0.5 and 4 %, depending on the pion momentum. The number of target deuterons per cm^2, n_T, involves an estimate of the filling factor (0.5). ϵ_{corr}, which varies between 0.70 and 0.95, is a correction factor which takes into account effects of pion decays (before and after the scattering), straggling of the particles, and pion absorption. This correction factor was estimated using Monte Carlo methods with an uncertainty of 4% (10%) for larger (smaller) values of ϵ_{corr}. In Fig. 7 the absolute cross sections from the T_{20} experiment at 256 MeV are shown together with those from Refs. 9 and 12. The angular dependence and the absolute values of all data from this experiment were found to be in good agreement with the published cross sections. Note that only statistical uncertainties are shown. The systematic errors would increase the error bars to 10–15 %.

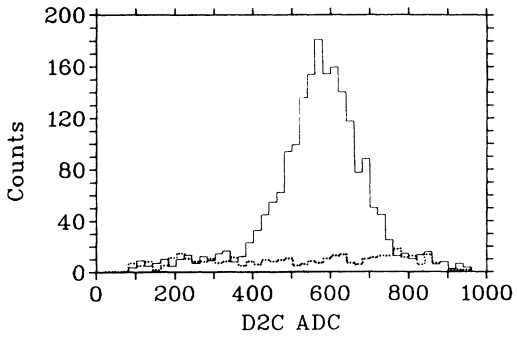

FIG. 6. Projection of the events in the polygon of Fig. 5 on the D_2 pulse height axis. The dotted line represents the results of a background target run normalized to the same number of incident pions as the foreground run.

B. Determination of T_{20} and τ_{21}

Three methods have been used to determine T_{20} and τ_{21} from the measured cross sections. We have called

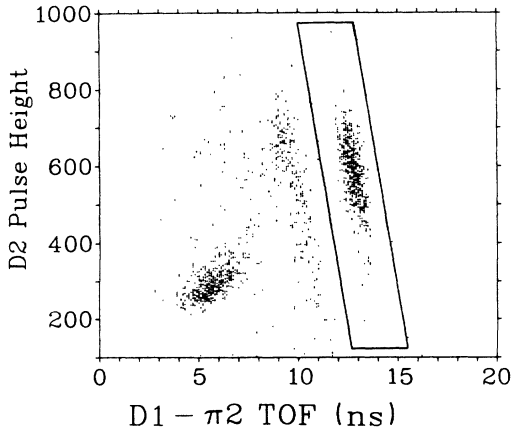

FIG. 5. Scatterplot of the events, for the T_{20} measurement at 256 MeV ($\theta_\pi = 150.6°$). Events inside the polygon are πd elastic and quasielastic (background) scattering events.

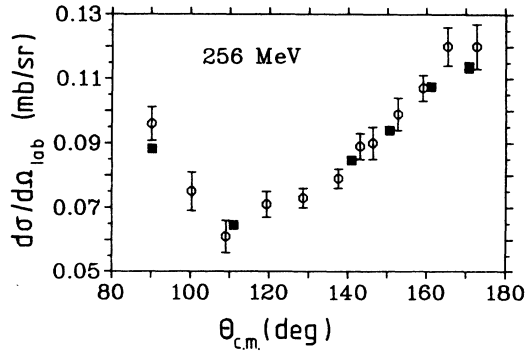

FIG. 7. Absolute differential cross section extracted from our measurements (solid squares) compared with those from Refs. 9 and 12 (open circles). Only statistical uncertainties have been included in the present results, the systematic errors are 10–15 %.

these the "fitting," "matrix," and "pair" methods. They are discussed below. They allow one to check the consistency of the relative cross sections with the corresponding tensor polarizations, and to compare the observables as determined from different cycles of the data taking sequence.

The fitting method is based on Eq. (1). The cross section σ^{pol} is a function of p_z and p_{zz}, where p_{zz} depends on p_z according to Eq. (2). Equation (1) can be rewritten

$$\sigma(p_z)=A+B\cdot p_z+C\cdot p_{zz} , \tag{3}$$

where

$$A=\sigma^0 ,$$

$$B=\sigma^0\cdot a_V\cdot iT_{11} ,$$

$$C=\sigma^0\cdot a_T\cdot T .$$

The coefficient a_T is $1/\sqrt{2}$ for the $T=T_{20}$ measurement, and $\sqrt{3}/2$ for the $T=\tau_{21}$ measurement. a_V should be zero for both measurements, and thus so should the coefficient B. Fitting the function of Eq. (3) to the measured relative cross sections for a given scattering angle and pion energy, the coefficients A, C, and, in general, B can be determined. The uncertainties in these coefficients are due to the statistical errors in the cross sections and can be calculated from the error matrix generated by the fitting routine. From these coefficients the observables can be calculated from:

$$iT_{11}=\frac{B}{a_V A}\ (a_V\neq 0) ,$$

$$\Delta iT_{11}=iT_{11}\cdot\left[\left[\frac{\Delta B}{B}\right]^2+\left[\frac{\Delta A}{A}\right]^2\right]^{1/2} ,$$

$$T=\frac{C}{a_T A} ,$$

$$\Delta T=T\cdot\left[\left[\frac{\Delta C}{C}\right]^2+\left[\frac{\Delta A}{A}\right]^2\right]^{1/2} .$$

In Fig. 8 the results of this fitting procedure for typical T_{20} and τ_{21} measurements are shown.

With this method a mean value for the observable is obtained, weighting the separate measurements according to their individual errors. Although the coefficient B should be zero, it may be added as free parameter in the fitting routine. If the fit requires $B\neq 0$, in a case where iT_{11} is small, this incidates that the determination of the target polarizations was in error. On the other hand, in a case where iT_{11} is large, $B\neq 0$ may also signal some misalignment of the target. For the measurements of T_{20} and τ_{21} reported here, B was always found to be consistent with zero.

The matrix method uses a different idea. If $p_z^{+(-)}$ refers only to the absolute value of p_z for positive (negative) polarization, then Eq. (3) can be rewritten for these polarizations as

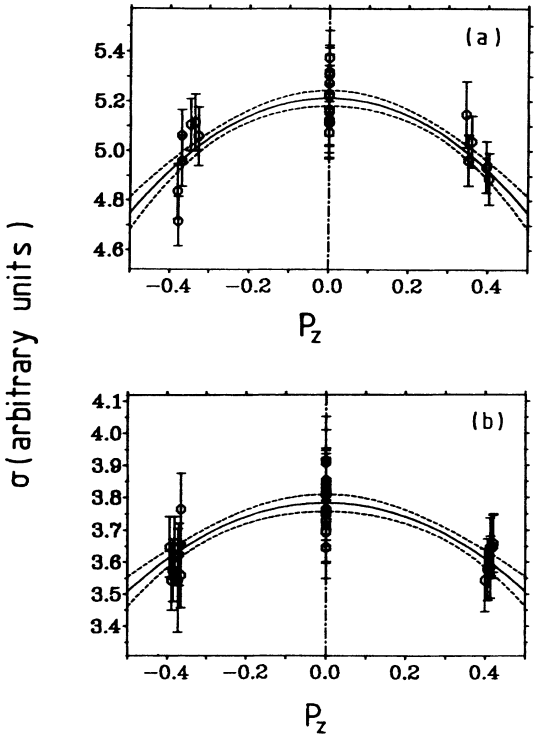

FIG. 8. Examples of fitting method using σ^+, σ^0, and σ^- data. The solid lines represent the best fit, and the dashed lines the associated error band. (a) is for the T_{20} measurement at 256 MeV ($\theta_\pi=171.7°$). The value obtained from the fit is $T_{20}=-0.793\pm 0.143$. (b) is for the τ_{21} measurement at 294 MeV ($\theta_\pi=155.2°$). The value obtained from the fit is $\tau_{21}=-0.497\pm 0.110$.

$$\sigma^+=\sigma^{0+}(1+a_V\cdot p_z^+\cdot iT_{11}+a_T\cdot p_{zz}^+\cdot T) , \tag{4}$$

$$\sigma^-=\sigma^{0-}(1-a_V\cdot p_z^-\cdot iT_{11}+a_T\cdot p_{zz}^-\cdot T) . \tag{5}$$

Here $p_{zz}^{+(-)}$ is the tensor polarization of the target, derived from $p_z^{+(-)}$, and $\sigma^{0+(-)}$ is the unpolarized cross section measured immediately before or after the corresponding polarized run in the sequences as defined above

$$\ldots,\sigma^+),(\sigma^+,\sigma^{0+}),(\sigma^{0-},\sigma^-),(\sigma^-,\ldots .$$

Adding and subtracting Eqs. (4) and (5), the following expressions are obtained:

$$a_T T=\frac{p_z^-(\sigma^+/\sigma^{0+})+p_z^+(\sigma^-/\sigma^{0-})-(p_z^++p_z^-)}{p_z^+p_{zz}^-+p_z^-p_{zz}^+} , \tag{6}$$

$$a_V iT_{11}=\frac{p_{zz}^-(\sigma^+/\sigma^{0+})-p_{zz}^+(\sigma^-/\sigma^{0-})+(p_{zz}^+-p_{zz}^-)}{p_z^+p_{zz}^-+p_z^-p_{zz}^+} , \tag{7}$$

where a_V, a_T, and T have the same meanings as above. Taking only the statistical uncertainties of the cross-section measurements, into account, the uncertainty in T can be calculated as

$$a_T\Delta T=\frac{\{(p_z^-/\sigma^{0+})^2[(\Delta\sigma^+)^2+(\sigma^+\Delta\sigma^{0+}/\sigma^{0+})^2]+(p_z^+/\sigma^{0-})^2[(\Delta\sigma^-)^2+(\sigma^-\Delta\sigma^{0-}/\sigma^{0-})^2]\}^{1/2}}{p_z^+p_{zz}^-+p_z^-p_{zz}^+} . \quad (8)$$

The analogous expression for $a_V\Delta IT_{11}$ can be obtained from the right-hand side of Eq. (8) by exchanging $p_z^{+(-)}$ with $p_{zz}^{+(-)}$ under the square root.

Making use of Eqs. (6) and (7), quadratic matrices can be constructed. The elements of these matrices, a_TT (a_ViT_{11}), were calculated from each pair of relative cross sections (polarized and associated unpolarized one) for both polarities. The diagonals of these matrices represent values of a_TT (a_ViT_{11}) from the time-ordered sequence of the $(\sigma^+,\sigma^{0+}),(\sigma^{0-},\sigma^-)$ measurements. The weighted averages for the respective observable at the given angle were determined from these diagonal elements. The off-diagonal elements were used as checks for possible systematic errors, because there the calculations of the observables are based on cross-section pairs not correlated by time order. This procedure made it possible to easily verify the consistency of the individual measurements. In Fig. 9(a), a graphical presentation of a matrix for the T_{20} measurement for a pion bombarding energy of 294 MeV and a scattering angle of 151.0° is shown. Figure 9(b) shows the individual results for the diagonal elements.

The major advantage of this method is the possibility to identify and eliminate errors from drifts in the electronics of the system. Therefore, only statistical errors were included in the error analysis. Furthermore, by comparing the results of a_ViT_{11} with zero, it is possible to perform the same tests of the alignment and determination of the polarizations, as described for the fitting method. A drawback of this method is that, due to the splitting of the sequence of cross sections in subclusters, the influence of each individual cross section on the calculated average is weighted also by the statistics of the other cross sections in that subcluster.

The pair method is the simplest of the three methods. As pointed out before, only one polarity of the target polarization is required for the determination of T_{20} and τ_{21}. This assumes that the direction of the target magnetic field is well aligned in the scattering plane. Therefore, $a_V=0$ and Eq. (3) can be written as:

$$T=\frac{1}{a_T}\frac{1}{p_{zz}}\left[\frac{\sigma^{\rm pol}}{\sigma^0}-1\right],$$

where T and a_T are presented in Table I. Taking only the statistical uncertainties of the cross-section measurements into account, the error in T is determined by:

$$\Delta T=\frac{1}{a_Tp_{zz}\sigma^0}\left[(\Delta\sigma^{\rm pol})^2+\left[\frac{\sigma^{\rm pol}}{\sigma^0}\Delta\sigma^0\right]^2\right]^{1/2} .$$

Using the subclustering of the sequence for the cross-section measurements, as described for the matrix method, a deduction of T from each individual pair $(\sigma^{\rm pol},\sigma^0)$ of polarized (positive or negative) and the associated unpolarized cross section was possible. By averaging the individual results separately for each polarity, two results for T were obtained. A disagreement between these results would indicate that the relative determination of the positive and negative polarization values was incorrect, or the alignment was in error. In this experiment, both results for T agreed. As in the case of the matrix method, in this analysis possible errors from drifts in

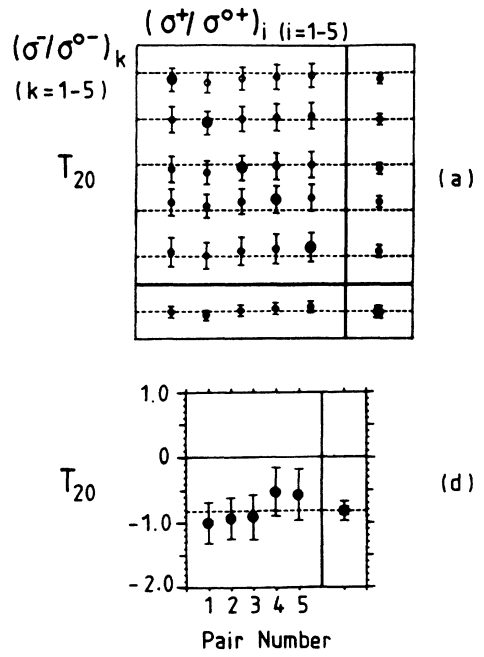

FIG. 9. (a) Graphical representation of a 5×5 matrix for the T_{20} measurement at 294 MeV (θ_π=151.0°). The elements of this matrix are calculated from the different $(\sigma^+/\sigma^{0+})_i(\sigma^-/\sigma^{0-})_k$ combinations. The diagonal elements correspond to the pairs in the sequence of the data taking. The sixth row (column) shows the average values of the five columns (rows). The dotted lines indicate the final averaged value which is shown in (b) $T_{20}=-0.823\pm0.155$.

TABLE I. T_{20} at 256 and 294 MeV.

T_π (MeV)	$\theta_{\rm c.m.}$	T_{20}
256	90.3	−0.44±0.15
	110.0	−0.19±0.17
	141.9	−0.68±0.14
	150.6	−0.98±0.13
	161.2	−0.75±0.13
	171.7	−0.77±0.13
294	91.1	−0.65±0.19
	110.8	−0.45±0.22
	142.4	−0.78±0.15
	151.0	−0.84±0.14
	161.0	−0.55±0.14
	171.8	−0.94±0.14

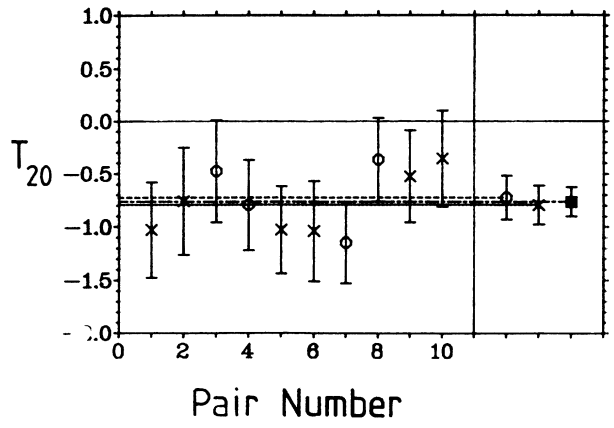

FIG. 10. Example of the pair method for the T_{20} measurement at 256 MeV ($\theta_\pi = 161.2°$). The T_{20} data represented by the open circles are obtained from (σ^+,σ^{0+}) pairs, those with a cross are obtained from (σ^-,σ^{0-}) pairs. To the right are average values for both polarities, and the mean value of these (solid square). The values obtained are $T_{20}^{+} = -0.72 \pm 0.21$, $T_{20}^{-} = -0.79 \pm 0.18$, and the mean $T_{20} = -0.76 \pm 0.14$.

the electronics during the data acquisition are suppressed. The final results for T were obtained from the weighted averages of the results for both polarities. Figure 10 shows an example of these results.

When comparing the results obtained by the three different methods, consistency was found for all angles and energies. Therefore, the mean value of these results was taken as the final result for T_{20} or τ_{21}. Since the three different methods produced very similar errors, the mean value of the three uncertainties was taken as the final error. Systematic uncertainties were shown to be negligible following the data reduction methods described above. Since all six pion scattering angles were measured simultaneously in this experiment, the error due to the absolute determination of p_{zz}, which is 8%, enters as an overall normalization uncertainty for the entire data set.

IV. RESULTS AND DISCUSSION

The experimental results are presented in Tables I and II. In Fig. 11 we compare the T_{20} data with theoretical

TABLE II. τ_{21} at 256 and 294 MeV.

T_π (MeV)	$\theta_{c.m.}$	τ_{21}
256	100.0	−0.38±0.09
	114.5	−0.49±0.10
	128.5	−0.66±0.10
	141.9	−0.52±0.09
	154.9	−0.41±0.09
	171.9	−0.21±0.11
294	100.8	−0.38±0.15
	115.3	−0.75±0.14
	129.1	−0.76±0.12
	142.4	−0.57±0.11
	155.2	−0.49±0.11
	171.9	−0.26±0.13

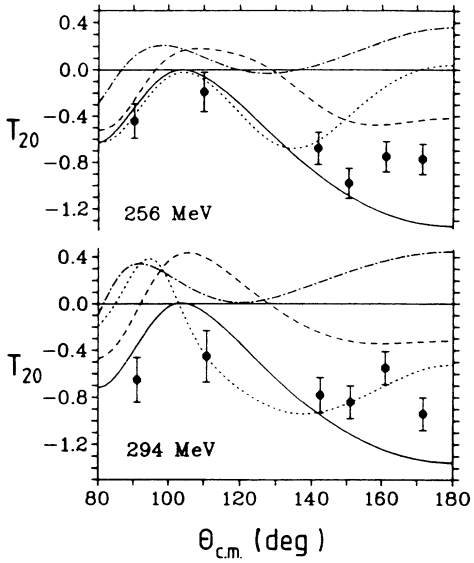

FIG. 11. Experimental results for T_{20} compared with theoretical predictions from Garcilazo (Ref. 23) (solid line), Hannover (Ref. 7) (dotted line), Flinders (Ref. 4) (dashed line), and Lyon (Ref. 35) (dot-dashed line).

predictions. From the many calculations available we show those from the Lyon group[34] (dot-dashed curve), from the Flinders group[4] (dashed curve), from Garcilazo[23] (solid curve) and from the Hannover group[7] (dotted curve). There are large variations in the predictions at backward angles. For an observable which does not depend on the interference of different helicity amplitudes (as in the case for the vector analyzing power iT_{11}) such a sensitivity to details of the theory is quite surprising.

The basic theoretical framework is similar, at least for the three Faddeev-type calculations. Therefore, the large discrepancies between the theories must be attributed to

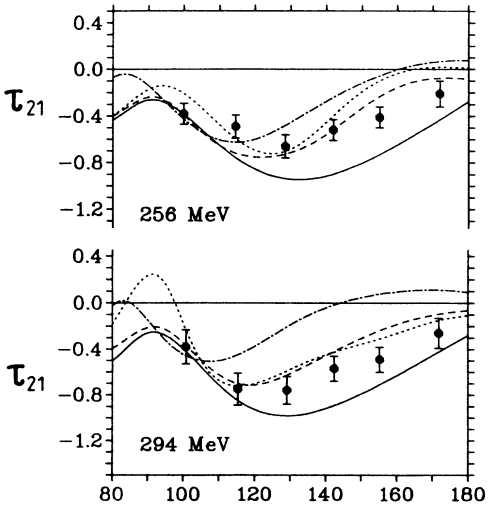

FIG. 12. Experimental results for τ_{21} compared with theoretical predictions. The lines are labeled as in Fig. 11.

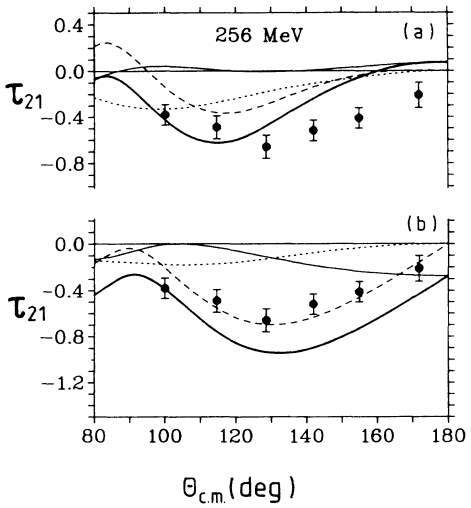

FIG. 13. Present results for τ_{21} at 256 MeV compared with predictions from (a) the Lyon group (Ref. 35) and (b) Garcilazo (Ref. 23). In both cases, the heavy solid line represents the full calculation for τ_{21}, the dashed line represents the contribution of T_{21}, the dotted line $T_{22}/2$, and the light solid line $T_{20}/2\sqrt{6}$.

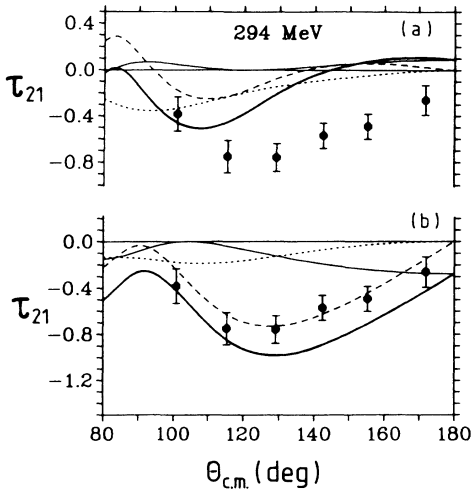

FIG. 14. Same as Fig. 13, but for 294 MeV.

the NN and/or the πN input used in each. For the NN input typically the $^3S_1 - {}^3D_1$ partial waves are used. The inclusion of heavy meson exchange in the NN sector showed very little effect on the observables in πd elastic scattering,[34] which may be explained by the fact that, in the Δ resonance region, this channel is dominated by the 2^+ partial wave, while the influence of the heavy meson exchange is only noticeable in the 0^+ wave which is not a dominant contribution. Also the NN $^1S_0$, $^3P_0$, $^3P_1$, $^3P_2$, and $^1P_1$ partial waves have very little effect on the various observables.[35]

Therefore, it appears that the large discrepancies between the theoretical predictions must be due to the πN input. Comparing experiment and theory for t_{20}^{lab} (which at large angles is dominated by T_{20}) Ungricht *et al.*[19] showed that the discrepancies between the theories are mainly due to the particular way in which the P_{11} πN t matrix is treated. On the other hand the predictions almost coincide when this partial wave is omitted.

The tensor polarization also appears to be sensitive to off-shell effects. The Lyon group introduced off-shell modifications in the P_{33} and P_{11} πN channels.[34] The effects are strongly energy dependent. At 180 MeV, where they are most pronounced, the off-shell effects greatly improve the agreement with the t_{20}^{lab} data, but at 142 and 256 MeV the effect goes in the wrong direction.

On the basis of our T_{20} data alone one would give preference to Garcilazo's predictions, but this has to be put in perspective by comparing the various calculations with other observables. The prediction for T_{20} from the Hannover group differs in the angular and energy dependence from all Faddeev calculations, and surprisingly also from the calculation of Lee and Matsuyama,[36] whose model is similar to the one used by the Hannover group. On the other hand, the Hannover group reproduces the iT_{11} data reasonably well, which is not true for the calculation of Lee and Matsuyama. Finally, there are substantial discrepancies between the cross-section predictions of both groups. It would be very useful if the respective theory groups would trace the sources of their disagreement. This is presently being done among those groups which employ the Faddeev formalism.

When comparing in Fig. 12 the composite observable τ_{21} with the predictions from the different groups one should be cautious in drawing conclusions, since τ_{21} depends on all three tensor observables, T_{21}, T_{22}, and T_{20}. For example, the "correct" theoretical prediction of τ_{21} by the Flinders group must be the result of an "incorrect" prediction of T_{21} and/or T_{22}, because T_{20} is incorrectly predicted (see Fig. 11). A final conclusion must await the comparison with the extracted observables T_{21} and T_{22} in the following paper. In Figs. 13 and 14, a decomposition of τ_{21} is shown for the calculations of the Lyon group, and Garcilazo.

ACKNOWLEDGMENTS

The polarized target material was kindly provided by Dr. T. O. Niinikoski, European Organization for Nuclear Research (CERN). This work would have been impossible without the generous help and considerable skills of the staff of SIN. It was supported by the Bundesministerium für Forschung und Technologie of the Federal Republic of Germany.

[1]H. N. Pendleton, Phys. Rev. **131**, 1833 (1963).
[2]T. Mizutani *et al.*, Phys. Rev. C **24**, 2633 (1981).
[3]A. S. Rinat *et al.*, Nucl. Phys. **A364**, 486 (1981).
[4]I. R. Afnan and B. Blankleider, Phys. Rev. C **22**, 1638 (1980).
[5]H. Garcilazo, Phys. Rev. Lett. **45**, 780 (1980).
[6]M. Betz and T.-S. H. Lee, Phys. Rev. C **23**, 375 (1981).
[7]H. Pöpping, P. V. Sauer, and Zhang Xi-Zhen, Nucl. Phys. **A474**, 557 (1987).

[8]E. Pedroni *et al.*, Nucl. Phys. **A300**, 321 (1978).
[9]K. Gabathuler *et al.*, Nucl. Phys. **A350**, 253 (1980).
[10]R. C. Minehart *et al.*, Phys. Rev. Lett. **46**, 1185 (1981).
[11]A. Stanovnik *et al.*, Phys. Lett. **94B**, 323 (1980).
[12]C. R. Ottermann *et al.*, Phys. Rev. C **32**, 928 (1985).
[13]G. R. Smith *et al.*, Phys. Rev. C **29**, 2206 (1984).
[14]K. Kanai *et al.*, Prog. Theor. Phys. **62**, 153 (1979).
[15]K. Kubodera and M. P. Locher, Phys. Lett. **87B**, 169 (1979).
[16]E. Ferreira *et al.*, J. Phys. G **13**, L39 (1987).
[17]B. Blankleider, Nucl. Phys. **A463**, 77c (1987).
[18]R. J. Holt *et al.*, Phys. Rev. Lett. **43**, 1229 (1979); *ibid.* **47**, 472 (1981).
[19]E. Ungricht *et al.*, Phys. Rev. C **31**, 934 (1985).
[20]Y. M. Shin *et al.*, Phys. Rev. Lett. **55**, 2672 (1985).
[21]T. Mizutani *et al.*, Phys. Rev. C **24**, 2633 (1981).
[22]B. Blankleider and I. R. Afnan, Phys. Rev. C **24**, 1572 (1981).
[23]H. Garcilazo, Phys. Rev. Lett. **53**, 652 (1984).
[24]H. Garcilazo, Phys. Rev. C **35**, 1804 (1987).
[25]G. R. Smith *et al.*, Phys. Rev. Lett. **57**, 803 (1986).
[26]G. R. Smith *et al.*, Phys. Rev. C **35**, 2343 (1987).
[27]G. R. Smith *et al.*, Phys. Rev. C **38**, 251 (1988).
[28]*Proceedings of the 3rd International Symposium on Polarized Phenomena in Nuclear Reactions, Madison, 1970,* edited by H. H. Barschall and W. Haeberli (University of Wisconsin Press, Madison, 1971).
[29]V. Koenig and W. Gruebler, Nucl. Phys. **A148**, 380 (1970).
[30]G. R. Smith *et al.*, Phys. Rev. C **30**, 980 (1984).
[31]E. L. Mathie *et al.*, Phys. Lett. **154B**, 28 (1985); W. Gyles *et al.*, Phys. Rev. C **33**, 595 (1986).
[32]W. de Boer, CERN report, 1974.
[33]O. Hamada *et al.*, Nucl. Instrum. Methods **A189**, 561 (1981).
[34]G. H. Lamot *et al.*, Phys. Rev. C **35**, 239 (1987).
[35]C. Fayard, private communication.
[36]T.-S. H. Lee and A. Matsuyama, Phys. Rev. C **36**, 1459 (1987).